A Robust Hierarchical Microcapsule for Efficient Supercapacitors Bearing Ultrahigh Current Density of 300 A/g

Cheng Yang, Minjie Shi, Xuefeng Song*, Xiaofeng Zhao, Liping Zhao, Jing Liu, Peng Zhang, Lian Gao*

State Key Laboratory for Metallic Matrix Composite Materials, School of Materials Science and Engineering, Shanghai Jiao Tong University, Shanghai 200240, P. R. China

*E-mail: songxfeng@sjtu.edu.cn (X. F. Song); liangao@mail.sic.ac.cn (L. Gao)

Synthesis of ZIF-8-derived nanoporous carbon (NPC)

NPC is derived from a zeolitic imidazole metal–organic framework (ZIF-8). Typically, zinc acetate (48 mM) was added to a methanol solution containing polyvinyl pyrrolidone (PVP, K30) (0.4 mM) to obtain the PVP-modified $Zn(CH_3COO)_2$. 200 mL of the as-prepared PVP-modified $Zn(CH_3COO)_2$ solution and methanol solution of 2-Methylimidazole (160 mM,200 mL) were cooled to 4 ℃ for 1 h. Sequentially, the two solutions were mixed and incubated at room temperature for 24 hours. The ZIF-8 was obtained by centrifugation, washed with methanol, and dried under vacuum at 60 °C. Finally, the ZIF-8 crystals were calcined under nitrogen atmosphere at 900 ℃ for 5 hours to acquire ZIF-8-derived NPC.

The mass ratio of the positive electrode (NiS_x@NCV microcapsules) to

the negative electrode (NPC) was decided according to the well-known charge balance theory (Q_+=Q-). The charge stored (Q) by each electrode depends on the following equation:

$$Q=C\times\Delta V\times m. \quad (1)$$

In order to realize Q_+=Q-, the mass balancing can be expressed as follows:

$$m_+/m_-= (C_-\times\Delta V_-)/(C_+\times\Delta V_+). \quad (2)$$

Based on the above analysis of the specific capacitances and the potential windows of the NiS_x@NCV microcapsules and NPC from galvanostatic discharge curves in a three electrode cell, as shown in Figure 3 and 4, the optimal mass ratio between the two electrodes should be $m(NiS_x@NCV)/m(NPC)=0.5$ in the asymmetric supercapacitor cell. In each cell, the weight of NiS_x@NCV and NPC are 0.5 mg and 1 mg, respectively.

The specific capacitance, energy and power density of assembled ASCs were calculated from the galvanostatic discharge curve according to the two-electrode systematic calculation method:

$$C=4I\Delta t/m\Delta V \quad (3)$$

$$E=C(\Delta V)^2/7.2 \quad (4)$$

$$P=3600\cdot E/\Delta t \quad (5)$$

where C (F/g) is the specific capacitance, E (Wh/kg) is the energy density, P (W/kg) is the power density, I is the discharge current, Δt is the discharge

time, ΔV is the voltage variation during the discharge process after "IR drop", m (mg) is the electrode weight. Additionally, the electrochemical performances and specific capacitance of single NiS_x@NCV or NPC electrode are measured and calculated according to the three-electrode systematic method.

The ion diffusion coefficient, D, can be calculated from the Warburg region using the following equation:

$$D = \frac{R^2T^2}{2A^2n^4F^4C^2\sigma_\omega^2} \quad (1)$$

In eqn (1), R is the gas constant, T is the absolute temperature, F is the Faraday constant, n is the number of electrons transferred per molecule, A is the active surface area of the electrode, C_0 is the concentration of ions in the electrolyte (6 M KOH), D is the apparent ion diffusion coefficient, and σ_ω the Warburg factor, which is related to Z' and can be obtained from the slope of the fitting line of the EIS data at low frequencies according to eqn (2).

$$Z' = R_e + R_{ct} + \sigma_\omega \omega^{-1/2} \quad (2)$$

R_e is the resistance between electrode and electrolyte, R_{ct} is the charge transfer resistance, and σ_ω is the Warburg factor obtained from the slope of the fitting line in Randles plot. That is to say, the ion diffusion coefficient is mainly determined by the slope of the fitting line in Randles plot.

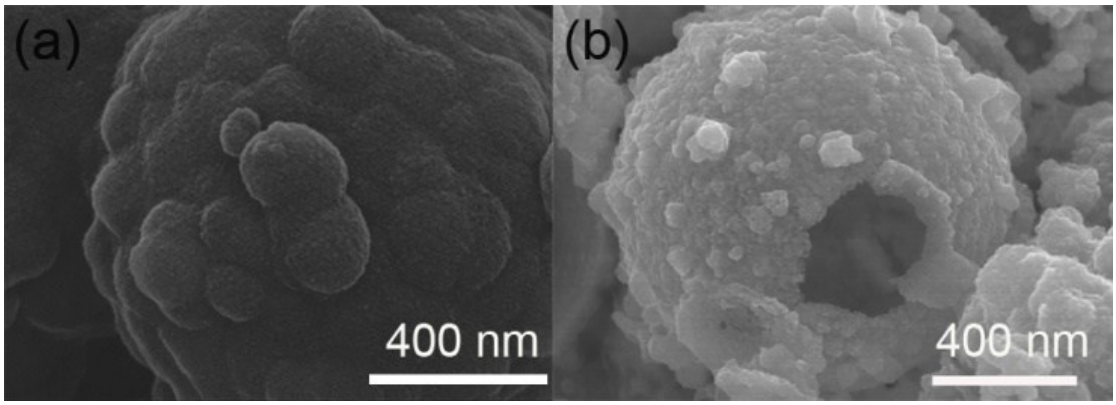

Fig. S1. FESEM images of (a) unbroken and (b) partially broken NiS_x@NCV microcapsules.

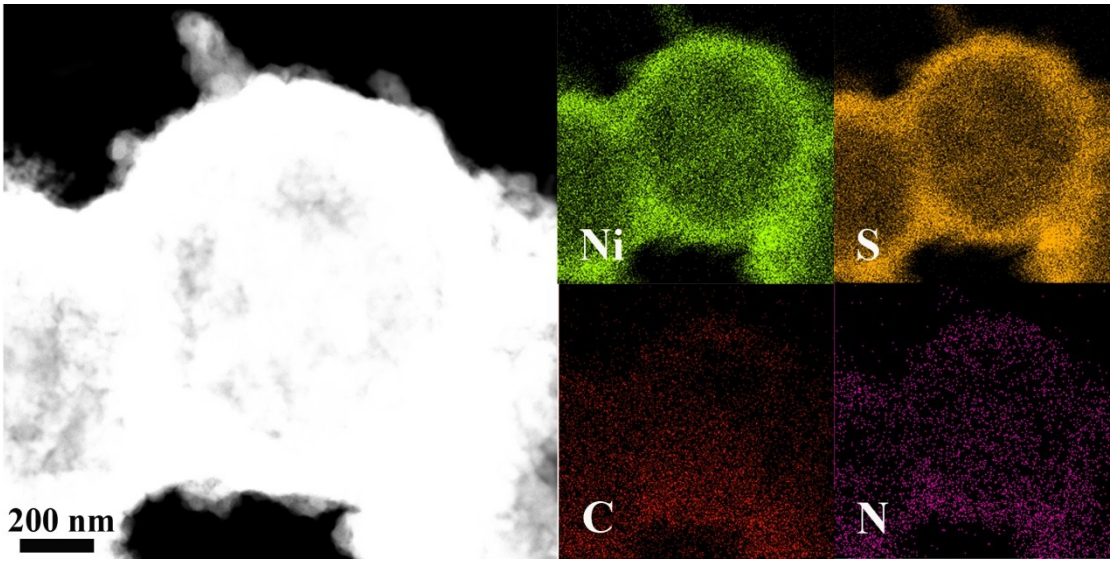

Fig. S2. Scanning transmission electron microscopy image of NiS_x@NCV microcapsules and corresponding elemental mapping images.

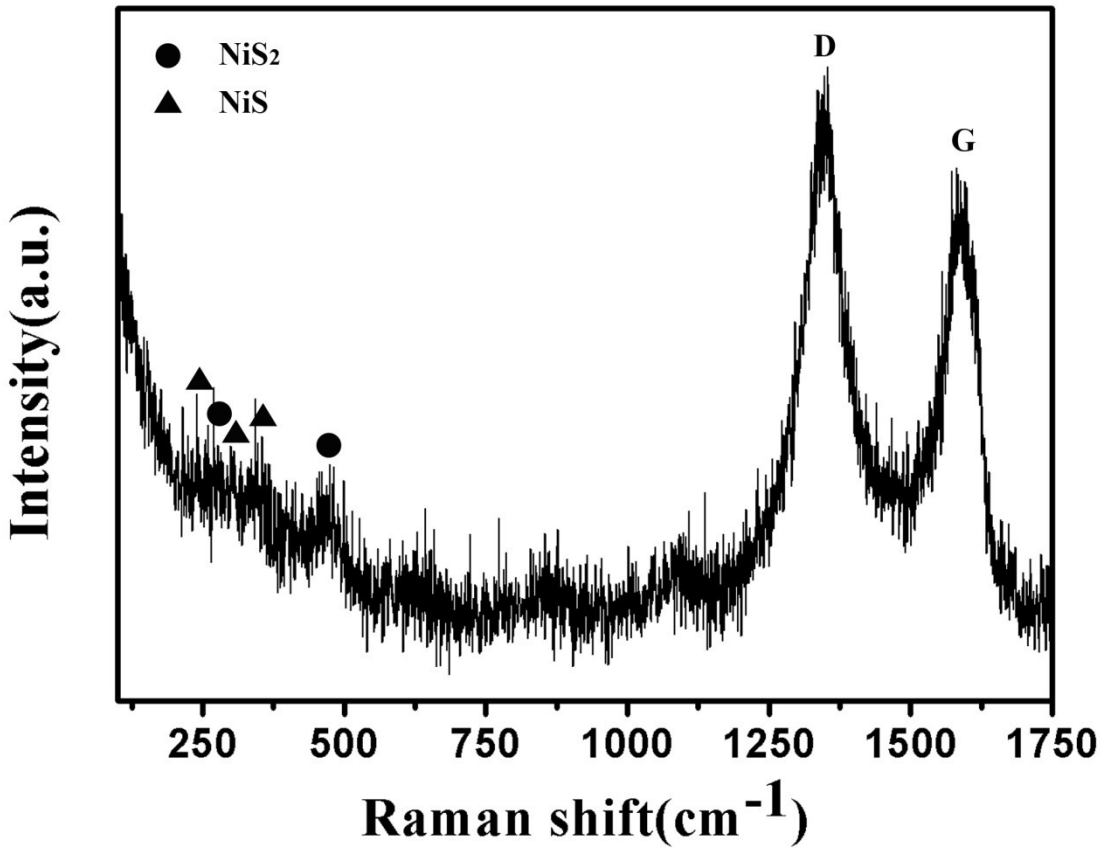

Fig. S3. Raman spectra of NiS_x@NCV microcapsules.

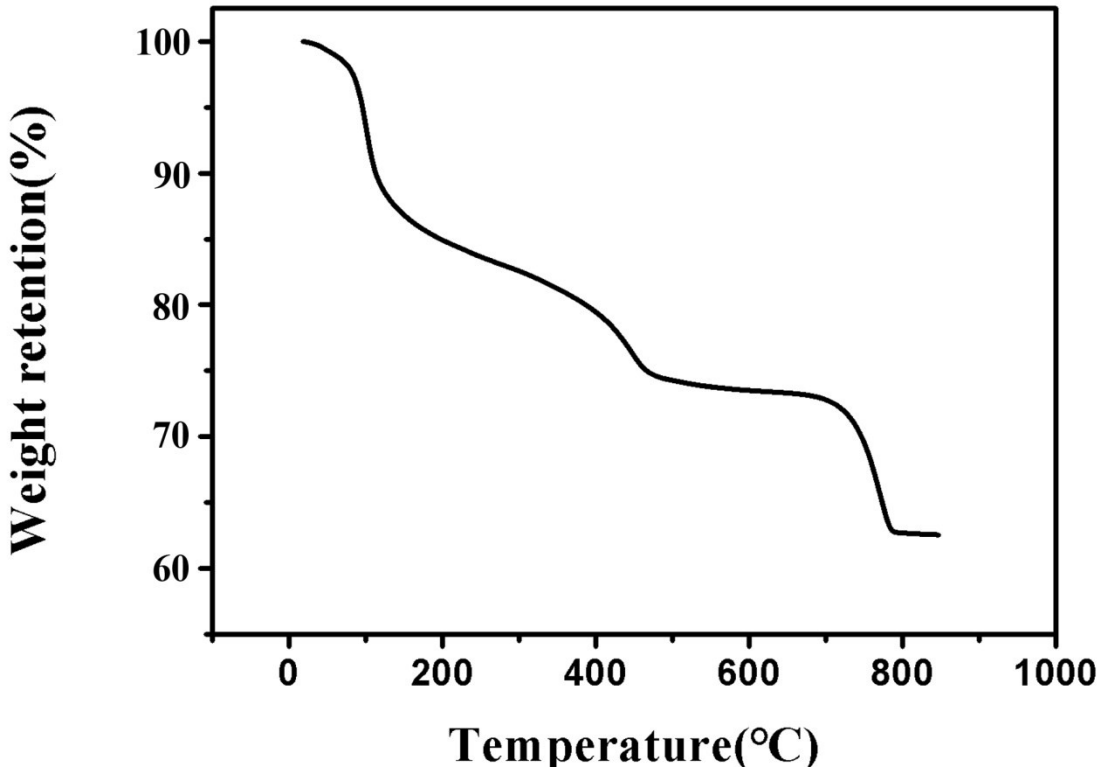

Fig. S4. TGA curves of NiS_x@NCV microcapsules ranging from 25 to 850 °C at a heating rate of 10°C /min under air flow.

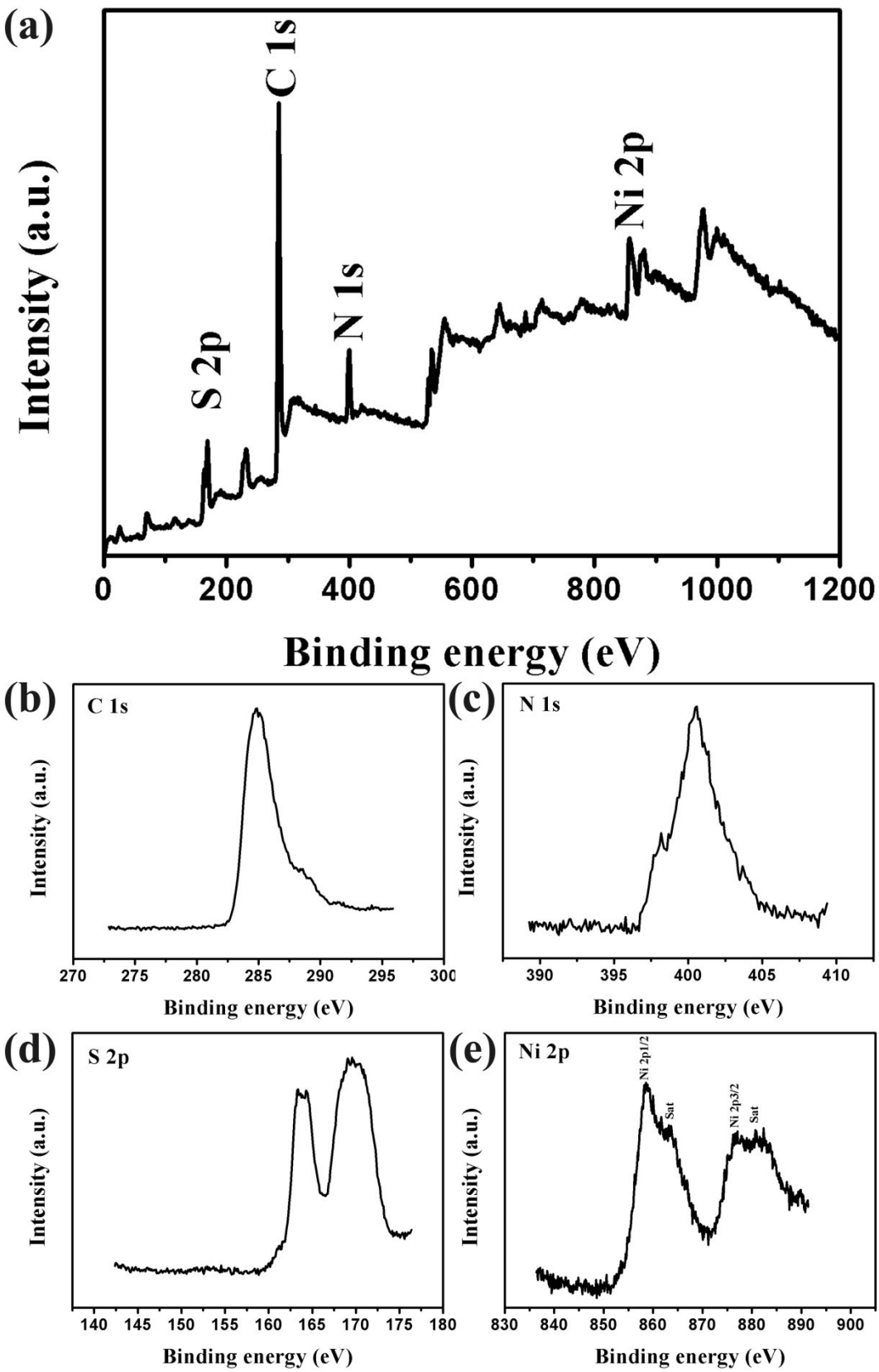

Fig. S5. (a)XPS survey spectra of NiS_x@NCV microcapsules, (b) the narrow spectra of C 1s, (c) the narrow spectra of N 1s, (d) the narrow spectra of S 2p, (e) the narrow spectra of Ni 2p. From characterization for the NiS_x@NCV, the C coating content, N doping content are 14.82% and 7.72%, respectively.

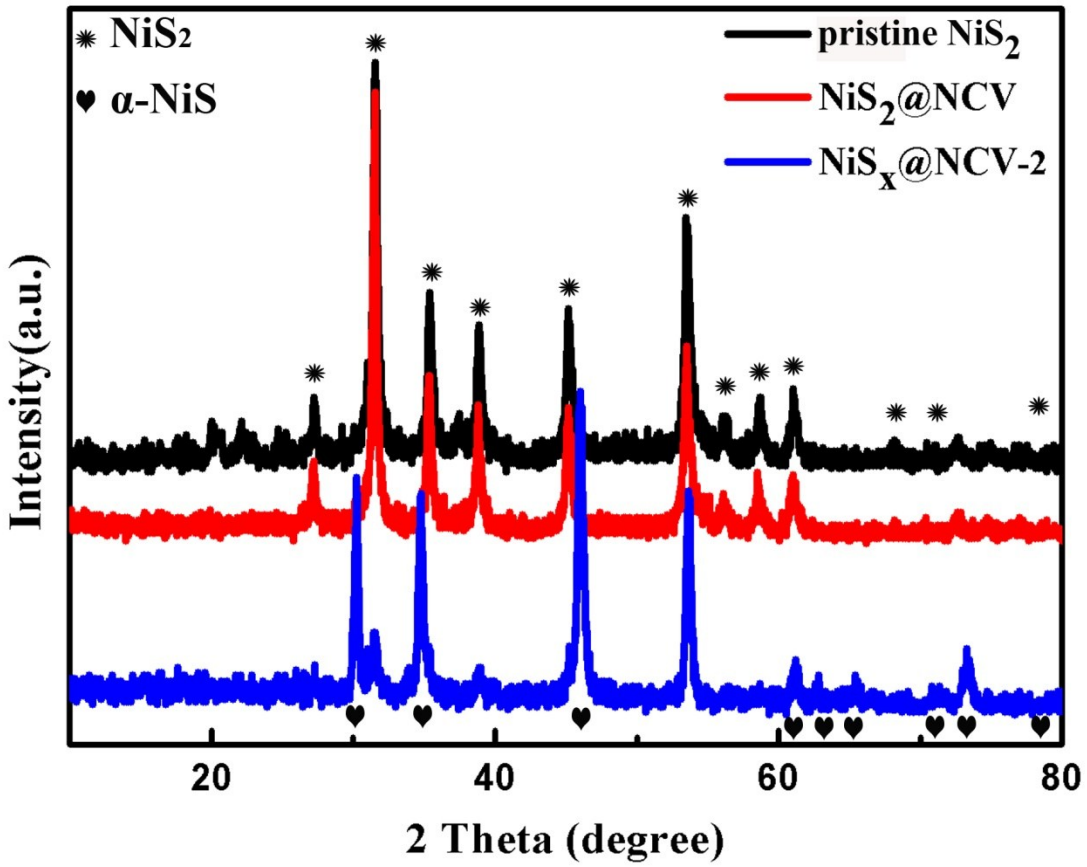

Fig. S6. XRD patterns of the pristine NiS_2, NiS_2@NCV and NiS_x@NCV-2.

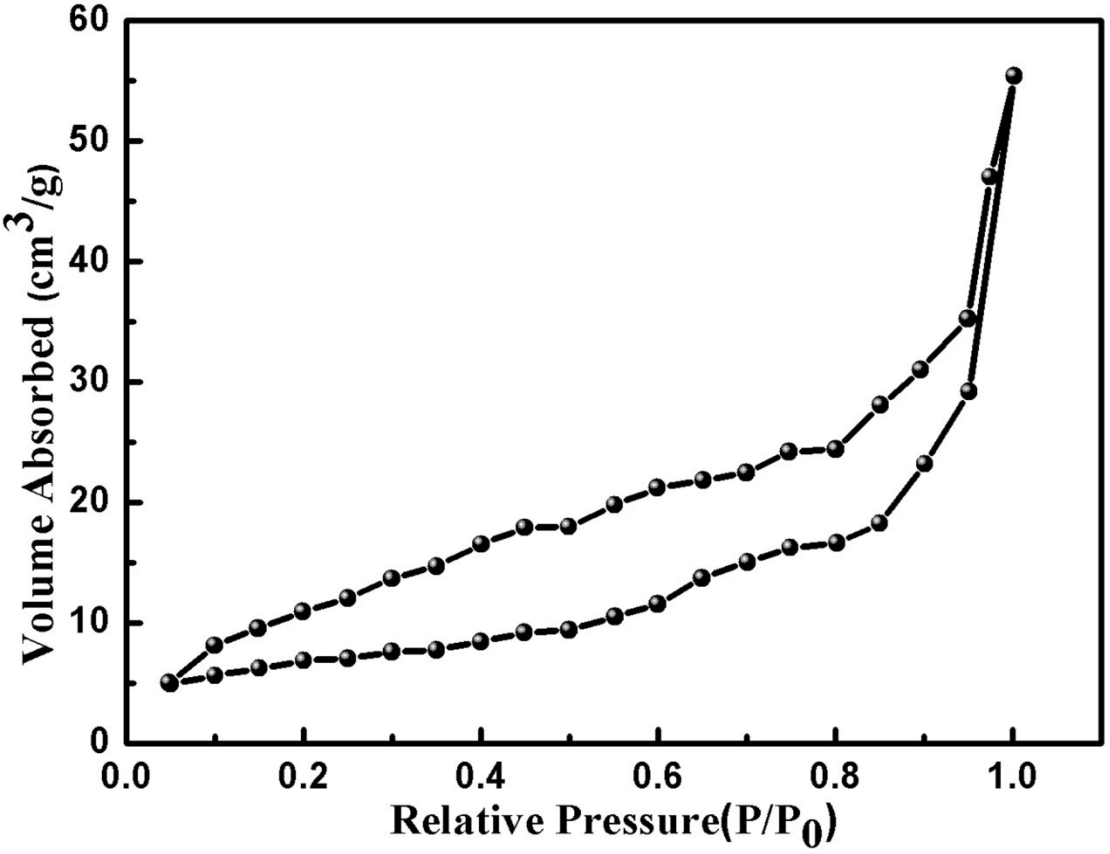

Fig. S7. Nitrogen adsorption/desorption isotherm of the pristine NiS_2. Pristine NiS_2 exhibits smaller specific surface area of 23.77 m^2/g and pore volume of 0.059 cm^3/g, which limits the accumulation of effective electron charges and ion diffusion during the electrochemical reaction.

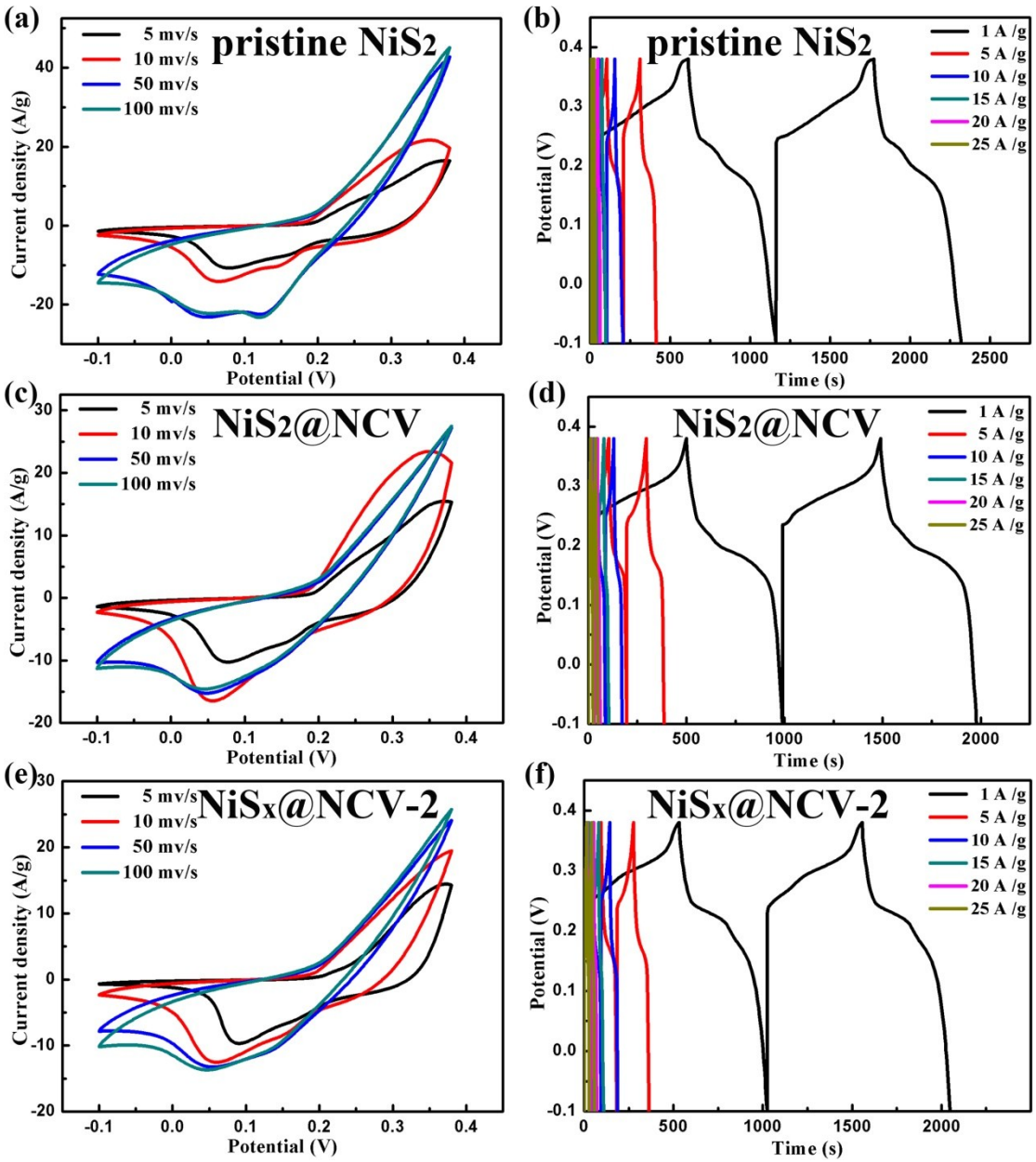

Fig. S8. (a)(c)(e) CV curves at various scan rates (5~100 mV/s) and (b) (d) (f) corresponding GCD curves at different current densities (1~25 A/g) of the pristine NiS_2 , NiS_2@NCV and NiS_x@NCV-2 electrodes, respectively. As the scan rate increases, the shapes of the CV curves of pristine NiS_2 and NiS_2@NCV become deformed, while the redox peaks become seriously shifted and even disappear, indicating that pristine NiS_2 and NiS_2@NCV have poor rate capability. As the annealing time prolonged, the amount of α-NiS increased while NiS_2 decreased within obtained NiS_x@NCV-2.

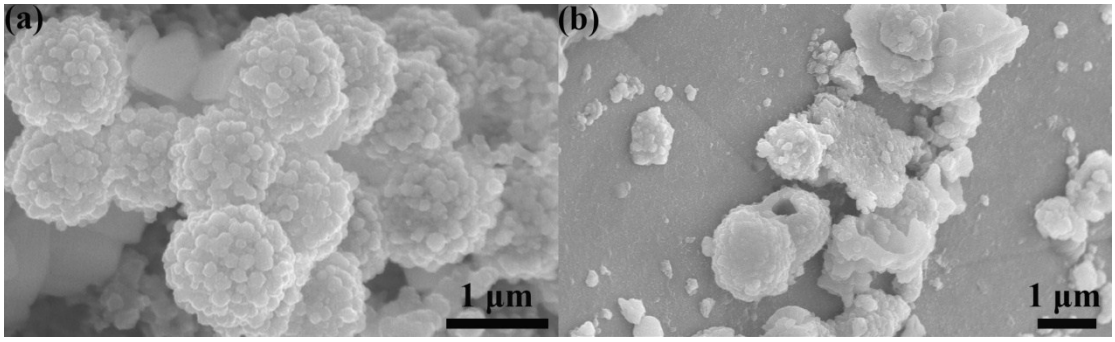

Fig. S9. FESEM images of (a) NiS_x@NCV and (b) pristine NiS_2 electrodes after 5 000 cycles at 1 A/g.

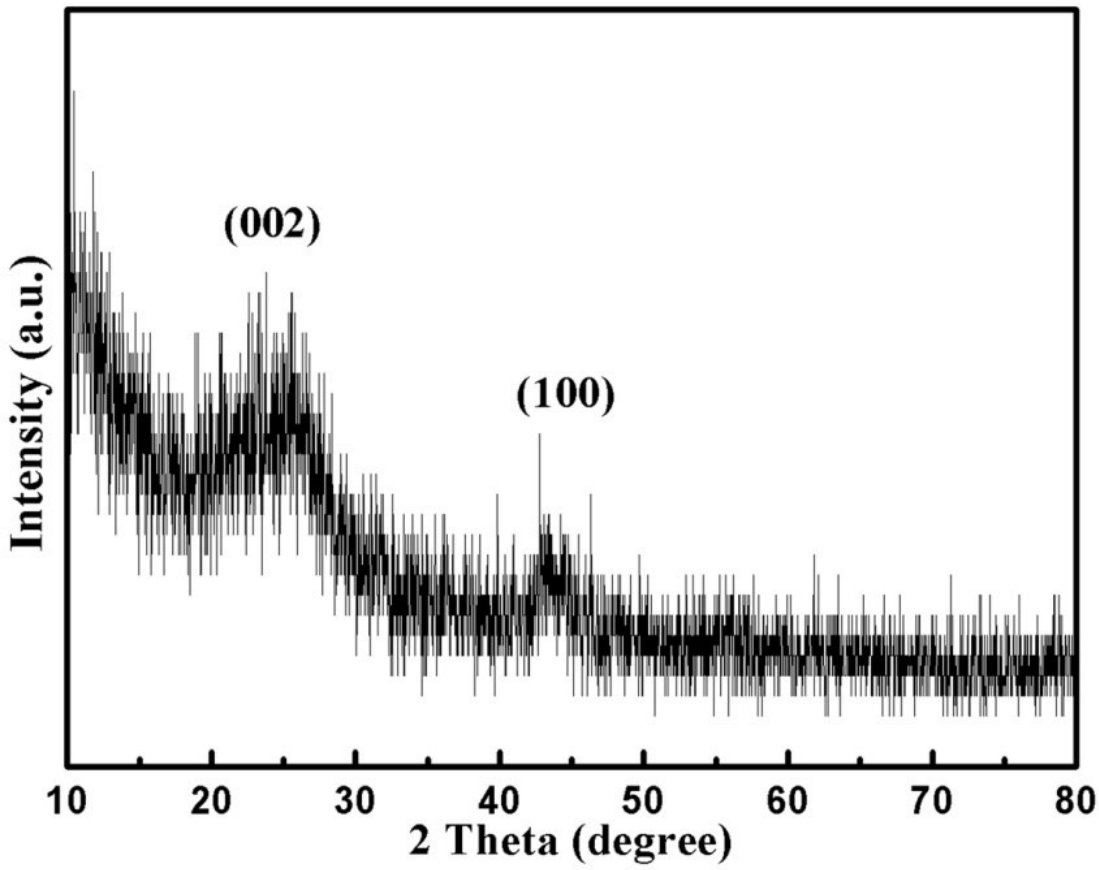

Fig. S10. XRD pattern of the nanoporous carbon particles.

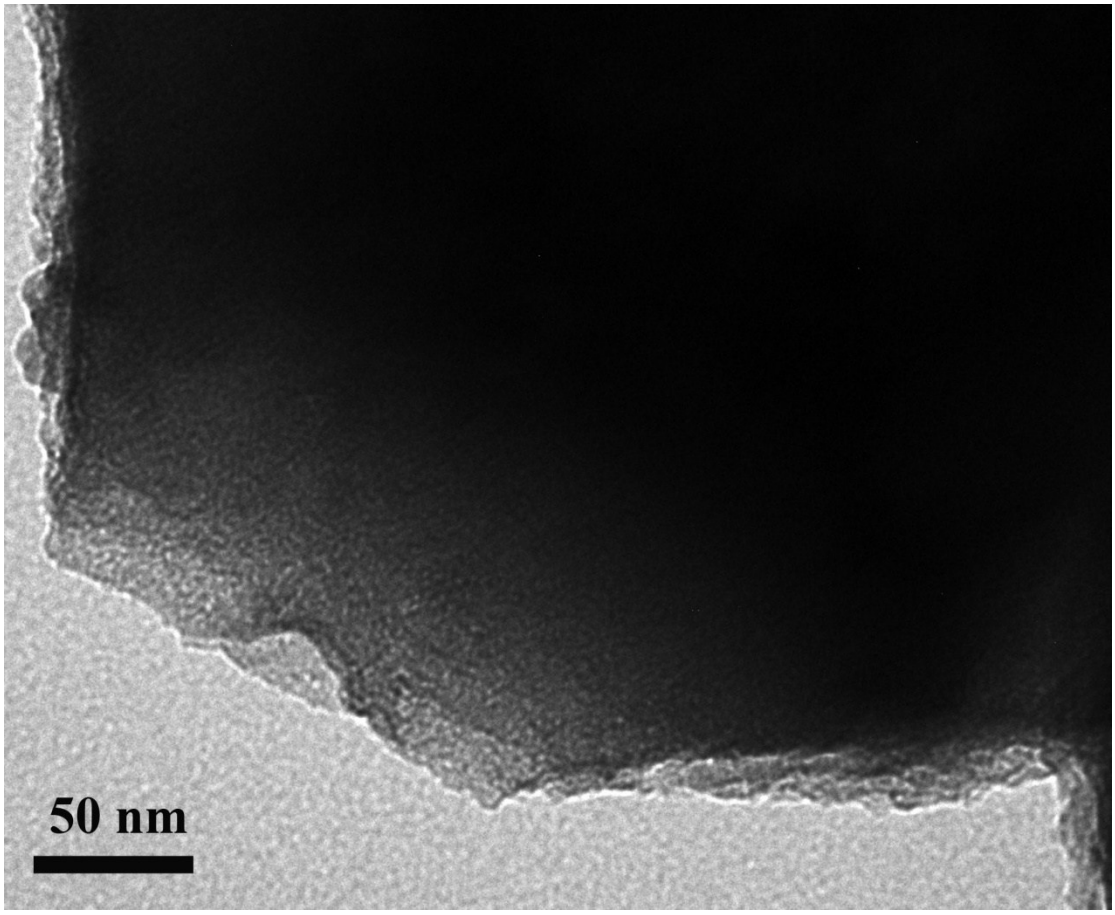

Fig. S11. TEM image on the edge of the NPC. There are abundant pores (~2.5 nm) existed in the carbon particles, which are easily accessible by electrolyte ions.

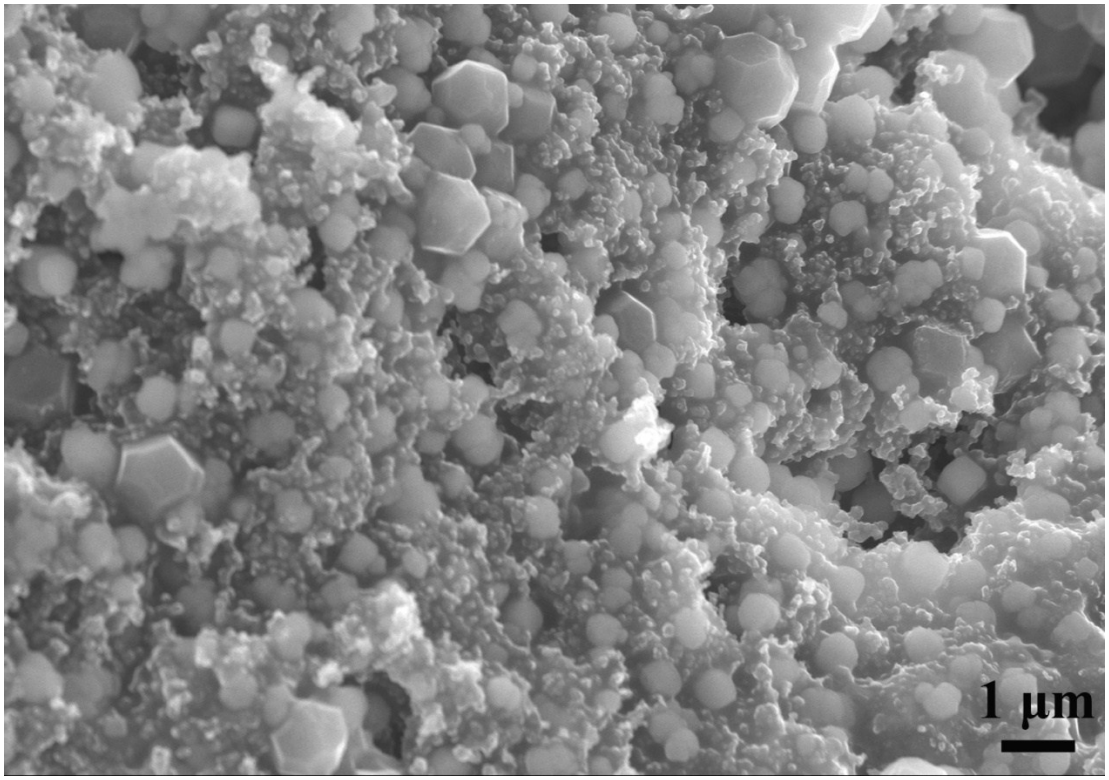

Fig. S12. FESEM image of the NPC electrode after 5000 cycles at 1 A/g.

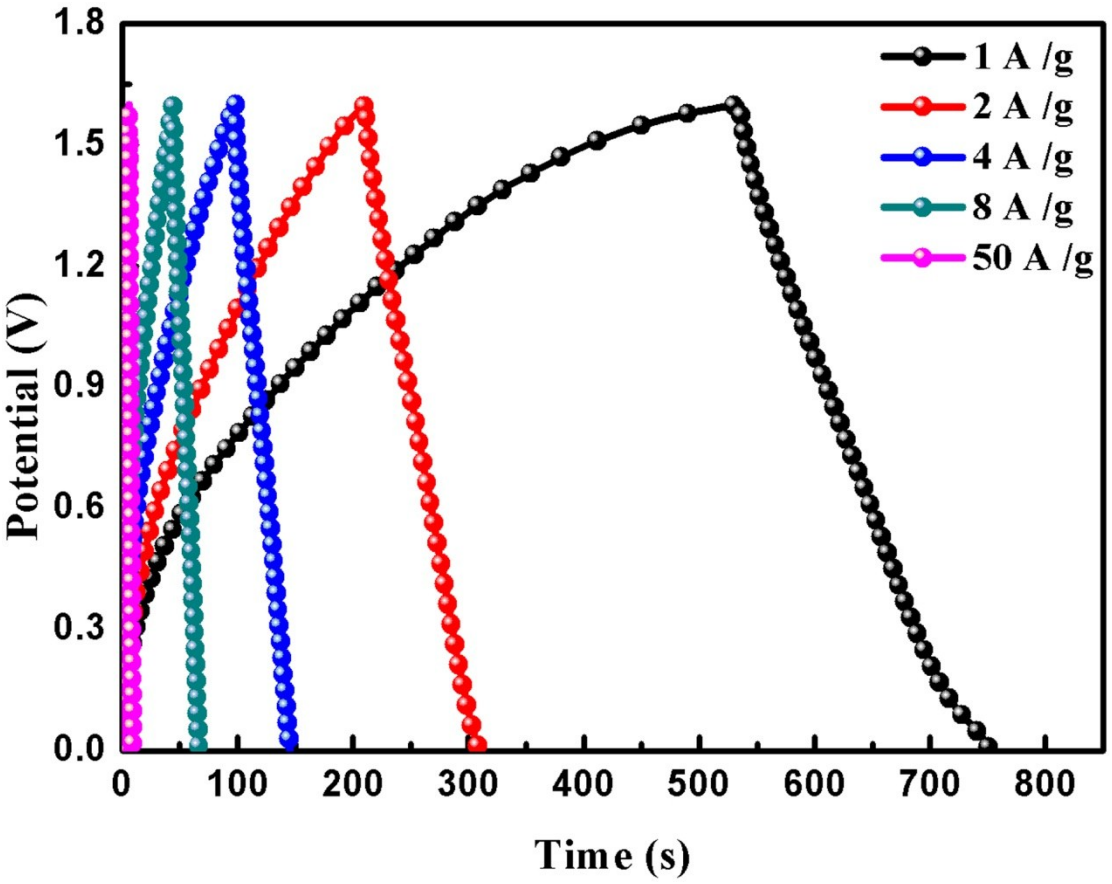

Fig. S13. The GCD curves at different current densities (1~50 A/g) of the NiS_x@NCV//NPC asymmetric supercapacitors.

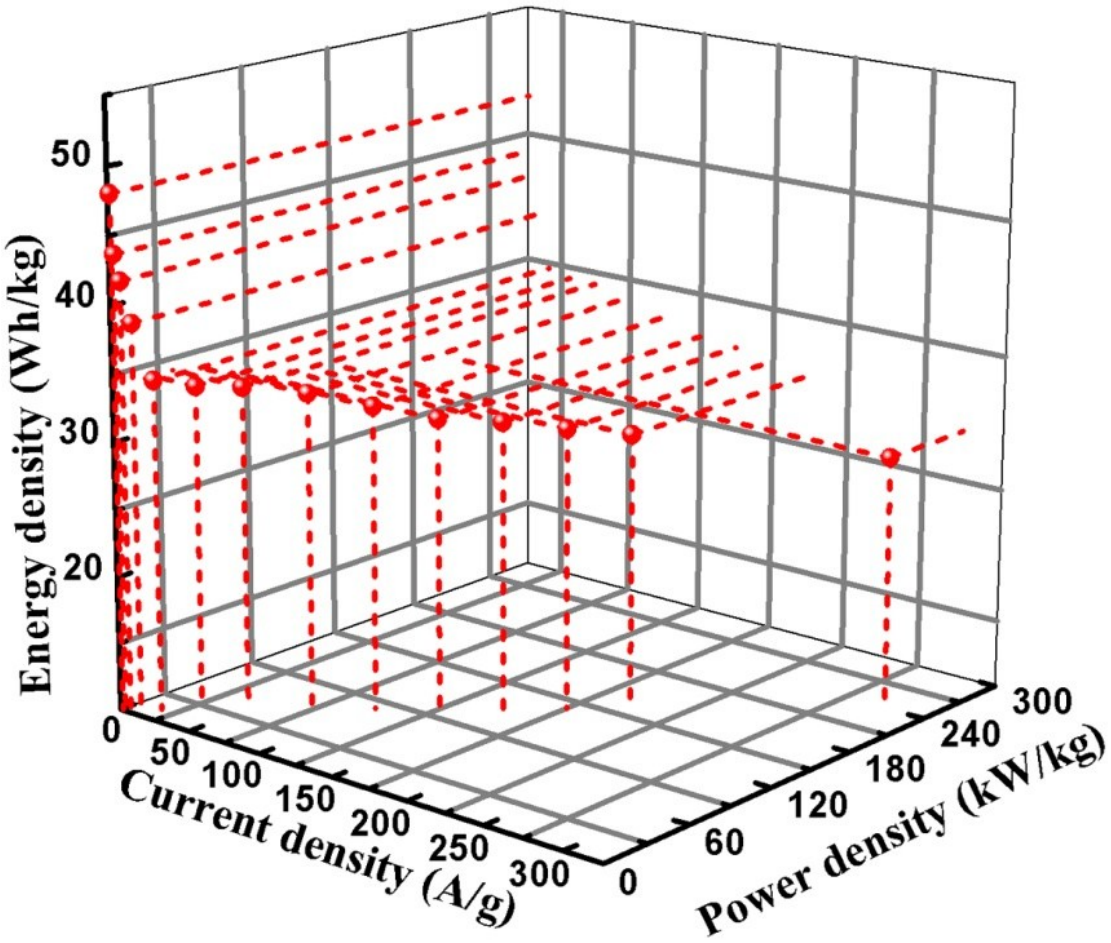

Fig. S14. The corresponding values of energy and power density under various current densities (1~300 A/g) of the NiS_x@NCV//NPC asymmetric supercapacitors.

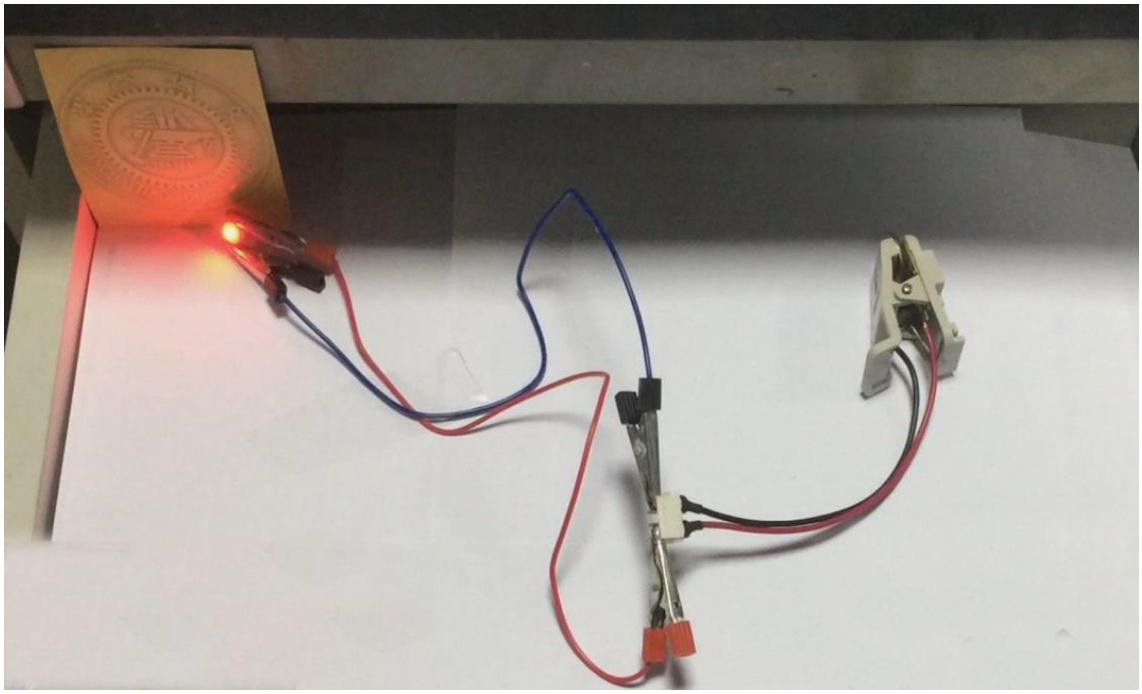

Fig. S15. Digital photo of the asymmetric SC. A red lamp can light up with the whole device.

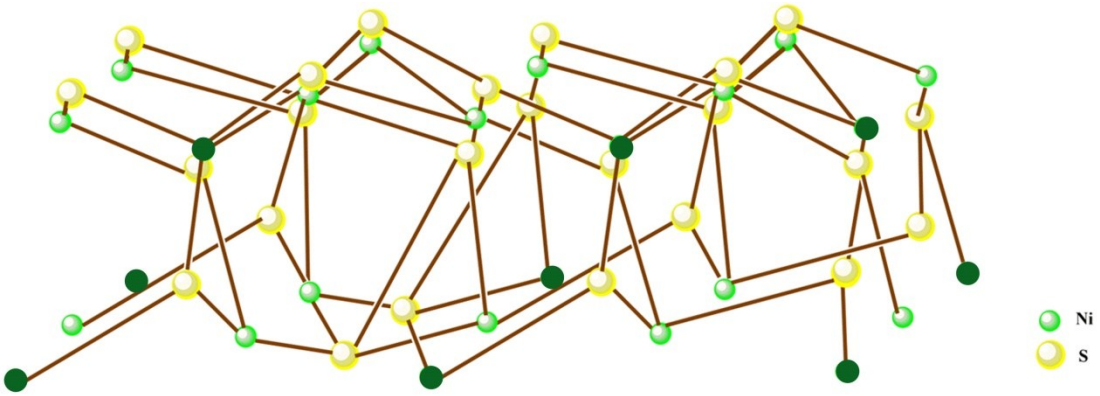

Fig. S16. The schematic crystal structure of the NiS_2 of projected based on data of ICSD-43717.The dark green balls denote Ni atoms exposed on the surface.

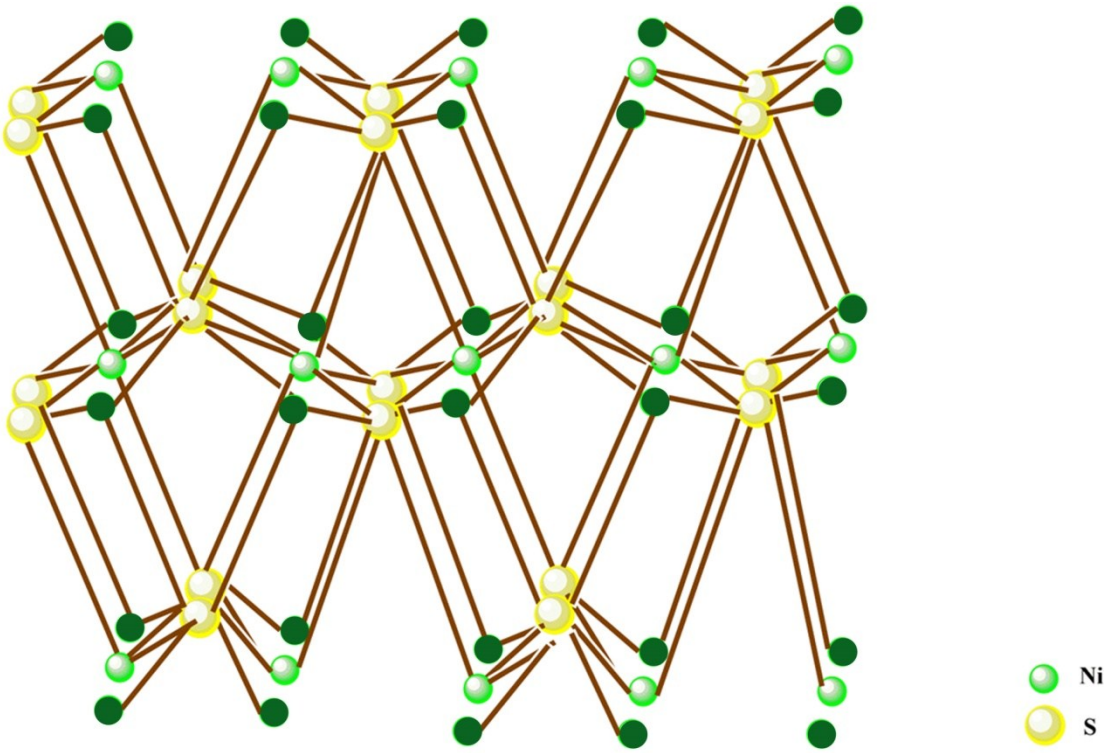

Fig. S17. The schematic crystal structure of the α-NiS of projected based on data of ICSD-42492. The dark green balls denote Ni atoms exposed on the surface.

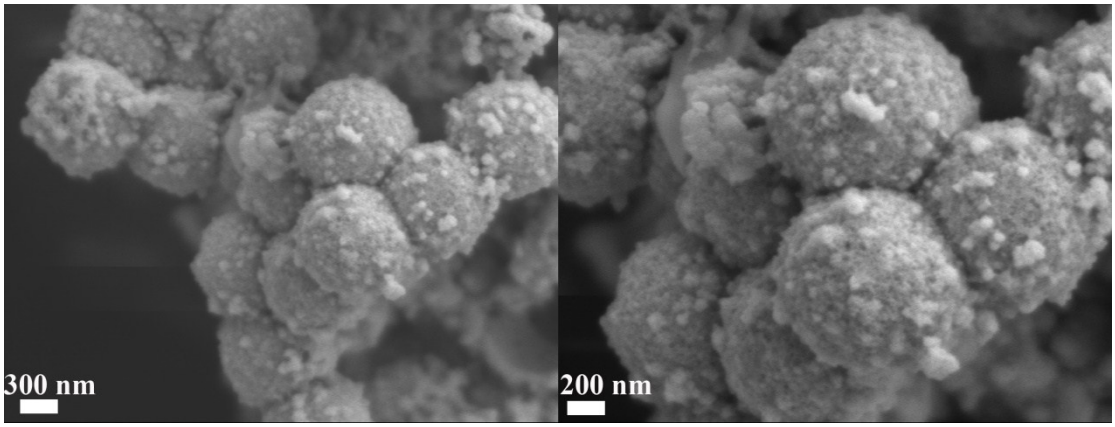

Fig. S18. FESEM images of NiS_x@NCV electrodes after 5 000 cycles at 300 A/g.

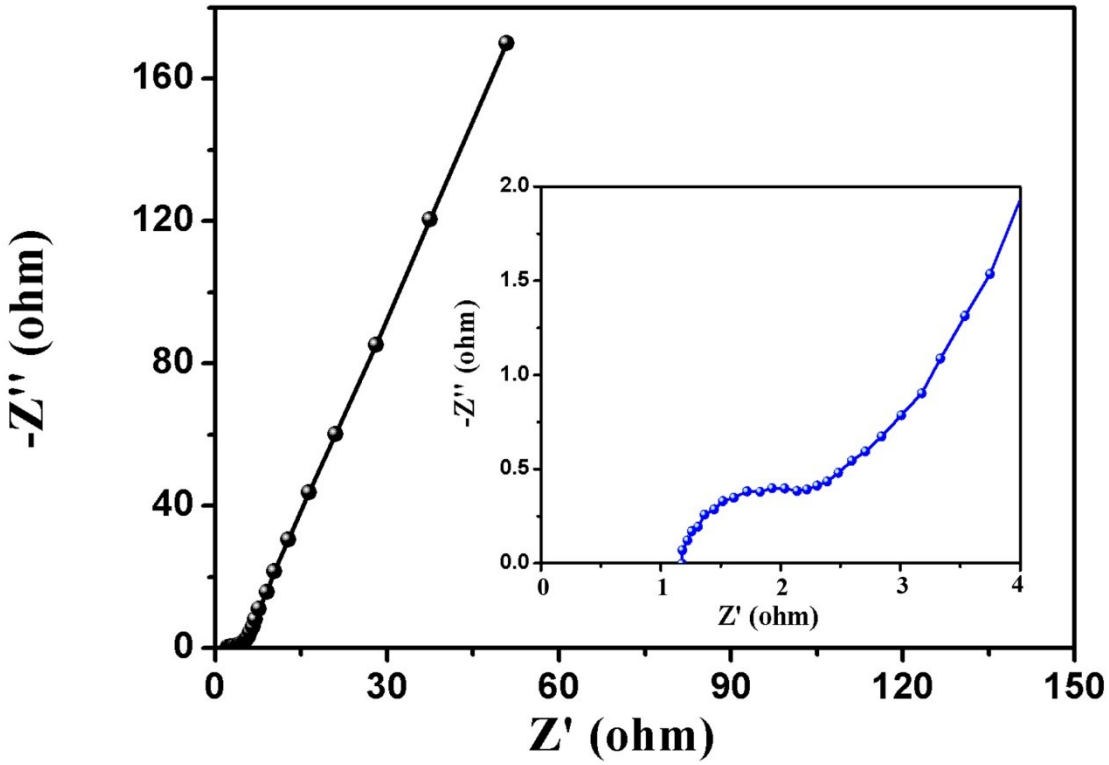

Fig. S19. EIS plot of NiS_x@NCV//NPC ASC after 5 000 cycles at 300 A/g.

Table S1. Comparision study of the rate capability between the NiS_x@NCV microcapsules electrode in this work and previously reported nickel sulfides based materials.

Materials	Capacitance (F/g)	Rate capability	Ref
NiS_2 nanocubes	695 (1.25 A/g)	22.7% (12.5 A/g)	[1]
NiS nanoframes	2112 (1 A/g)	33.6% (20 A/g)	[2]
NiS nanorods	1403.8 (1 A/g)	35.19% (10 A/g)	[3]
NiS microflowers	1122.7 (1 A/g)	41.4% (20 A/g)	[4]
Rod-like NiS_2	1020.2 (1 A/g)	52% (10 A/g)	[5]
NiS_2/ZnS	1198 (1 A/g)	49.3% (10 A/g)	[6]
Flower-like β-NiS	965.98 (0.5 A/g)	49% (10 A/g)	[7]
Ni_3S_2/MWCNT	1024 (0.8 A/g)	46.8% (25 A/g)	[8]
Ni_3S_4@MoS_2	1440.9 (2 A/g)	55% (20 A/g)	[9]
NiS_2/NiO	2251 (1 A/g)	48% (20 A/g)	[10]
CNT@Ni_3S_2	585 (1 A/g)	61.8% (13.3 A/g)	[11]
NiS hollow spheres	927 (4.08 A/g)	62.8% (10.2 A/g)	[12]
NiS/rGO aerogel	852 (2 A/g)	61.7% (15 A/g)	[13]
NiS/CRs	1092 (1 A/g)	67.7% (10 A/g)	[14]
NiS_2/CoS_2	954.3 (1 A/g)	32.4% (20 A/g)	[15]
NiS_x@NCV microcapsules	1600 (1 A/g)	84.25% (25 A/g)	This work

Table S2. Comparision study of the rate capability, energy density and power density between the NiS_x@NCV//NPC ASCs in this work and previously reported nickel sulfides based SCs.

Device	Rate capability	Energy density (Wh/kg)	Power density (KW/kg)	Ref
Ni_3S_2/MWCNT//AC	62.7% (16 A/g)	19.8	0.798	[8]
		11.03	12.1	
Rod-like NiS_2//rGO	36.1% (15 A/g)	32.76	0.954	[5]
		11.19	13.52	
NiS/NF//AC	32.4% (50 mA/cm^2)	38.4	0.1666	[16]
		11	3.9	
NiS microflower//AC	43.7% (10 A/g)	31	0.9	[4]
		12.9	8.8	
Ni_3S_2//AC	37.3% (2 A/g)	34.6	0.15	[17]
		12.9	1.5	
MCs@GNS@NiS	64.9% (5 A/g)	17.2	0.103	[18]
		11.2	1.008	
NiS_2-CoS_2//AC	45.7% (10 A/g)	29.3	0.7	[15]
		13.4	7.4	
NiS/RGO//AC	62.1% (4 A/g)	18.7	0.124	[13]
		11.6	2.9	
Ni_3S_2@β-NiS//AC	39.8% (30 A/g)	55.1	0.9259	[19]
		22.2	28.1	
NiS_2/ZnS//AC	68% (10 A/g)	28	0.7489	[6]
		19.4	7.509	
Ni_3S_2/CNF//CNF	62.5% (10 A/g)	25.8	0.425	[20]
		15.2	6.8	
NiS//ZIF-8 derived carbon	78% (9 A/g)	17.01	2.28	[21]
		13.42	10.283	
NiS_x@NCV//NPC	87% (300 A/g)	48.02	0.8	This work
		30	240	

References

[1] H. Pang, C. Wei, X. Li, G. Li, Y. Ma, S. Li, J. Chen, J. Zhang, Sci. Rep. 4 (2014).

[2] X. Y. Yu, L. Yu, H. B. Wu, X. W. Lou, Angew. Chem. Int. Ed. 54 (2015) 5331-5335.

[3] Z. Wang, C. Nan, D. Wang, Y. Li, Rsc Adv. 4 (2014) 47513-47516.

[4] B. Guan, Y. Li, B. Yin, K. Liu, D. Wang, H. Zhang, C. Cheng, Chem. Eng. J. 308 (2017) 1165-1173.

[5] Y. Ruan, J. Jiang, H. Wan, X. Ji, L. Miao, L. Peng, B. Zhang, L. Lv, J. Liu, J. Power Sources 301 (2016) 122-130.

[6] G. C. Li, M. Liu, M. K. Wu, P.-F. Liu, Z. Zhou, S. R. Zhu, R. Liu, L. Han, Rsc Adv. 6 (2016) 103517-103522.

[7] J. Yang, X. Duan, Q. Qin, W. Zheng, J. Mater. Chem. A 1 (2013) 7880-7884.

[8] C. S. Dai, P. Y. Chien, J. Y. Lin, S. W. Chou, W. K. Wu, P. H. Li, K. Y. Wu, T. W. Lin, Acs Appl. Mater. Interfaces 5 (2013) 12168-12174.

[9] Y. Zhang, W. Sun, X. Rui, B. Li, H.T. Tan, G. Guo, S. Madhavi, Y. Zong, Q. Yan, Small 11 (2015) 3694-3702.

[10] D. Zhang, X. Zhou, K. Ye, Y. Li, C. Song, K. Cheng, D. Cao, G. Wang, Q. Li, Electrochim. Acta 173 (2015) 209-214.

[11] T. Zhu, H.B. Wu, Y. Wang, R. Xu, X.W. Lou, Adv. Energy Mater. 2 (2012) 1497-1502.

[12] T. Zhu, Z. Wang, S. Ding, J. S. Chen, X. W. Lou, Rsc Adv. 1 (2011) 397-400.

[13] F. Cai, R. Sun, Y. Kang, H. Chen, M. Chen, Q. Li, Rsc Adv. 5 (2015) 23073-23079.

[14] C. Sun, M. Ma, J. Yang, Y. Zhang, P. Chen, W. Huang, X. Dong, Sci. Rep. 4 (2014).

[15] H. Zhang, B. Guan, J. Gu, Y. Li, C. Ma, J. Zhao, T. Wang, C. Cheng, Rsc Adv. 6 (2016) 58916-58924.

[16] L. Yu, B. Yang, Q. Liu, J. Liu, X. Wang, D. Song, J. Wang, X. Jing, J. Electroanal. Chem. 739 (2015) 156-163.

[17] H. H. Huo, Y. Q. Zhao, C. L. Xu, J. Mater. Chem. A 2 (2014) 15111-15117.

[18] Y. Li, K. Ye, K. Cheng, J. Yin, D. Cao, G. Wang, J. Power Sources 274 (2015) 943-950.

[19] W. Li, S. Wang, L. Xin, M. Wu, X. Lou, J. Mater. Chem. A 4 (2016) 7700-7709.

[20] W. D. Yu, W. R. Lin, X. F. Shao, Z. X. Hu, R. C. Li, D. S. Yuan, J. Power Sources 272 (2014) 137-143.

[21] P. R. Jothi, R. R. Salunkhe, M. Pramanik, S. Kannan, Y. Yamauchi, Rsc Adv. 6 (2016) 21246-21253.